Fachtagung "Experimentelle Strömungsmechanik"
5.–7. September 2023, München

Stereoscopic Measurements of Blade Deformation on a Shrouded Prop-Fan with Boundary Layer Ingestion by means of Image Pattern Correlation Technique

Stereoskopische Messungen der Schaufeldeformation des Rotors eines ummantelten Fans mit Grenzschichteinsaugung mit der Image Pattern Correlation Technik

J. Klinner, M. Schroll, M. Voges, C. Willert
Deutsches Zentrum für Luft- und Raumfahrt, Insitut für Antriebstechnik, Linder Höhe, 51147 Köln, Corresponding Author: joachim.klinner@dlr.de

Schlagworte: Schaufeldeformation, IPCT, Turbomaschine, Grenzschichteinsaugung
Keywords: blade deformation measurements, IPCT, turbomachine, boundary layer ingestion

Abstract

The material presented herein describes the implementation of optical blade deformation measurements based on the image pattern correlation technique (IPCT) in a stereoscopic imaging configuration applied to the first rotor of a counter-rotating shrouded fan stage (CRISPMulti) which has a diameter of about 1m. The correlation-based stereoscopic image analysis is discussed, as well as the difficulties with regard to the correlation-based stereo matching of two camera views for the highly curved blade surface involving pattern displacements up to 12% of the image height. Cross-correlation of speckle images at reference position with images of the displaced positions recovered the full 3c displacement field in the optically assessable area of the suction side. The three-dimensional displacements could be evaluated with triangulation errors below 0.5mm at blade tip velocities exceeding 250m/s (4830rpm). Comparative measurements using a third camera imaging the blade tip match the stereo IPCT results within deviations of 0.5mm for the axial component whereby the circumference component matches closely.

Introduction

Boundary layer ingestion (BLI) propulsion systems have gained much attention because of their potential to significantly reduce the fuel consumption of future civil aircrafts. On the other hand, the rotor blades are subjected to periodical inlet disturbances involving low-engine-order excitations at large dynamical loads [Eichner and Belz 2019]. Within the internal DLR project AGATA3S the influence of such boundary layer (BL) disturbances is investigated on a dedicated counter-rotating shrouded fan stage (CRISPMulti), whose blading is made of reinforced composites [Aulich et al. 2013; Schmid et al. 2019; Lengyel-Kampmann et al. 2023].
Measurements of static and dynamic deformations of the blading of rotor no.1 are needed to provide comparative data for coupled flow-structure simulations. The Image Pattern Correlation Technique (IPCT) [Boden and Stasicki 2014, Kirmse et al. 2016] was implemented to measure aeroelastic deformations of a blade of the first rotor from the CRISPMulti at different circumferential positions of inlet disturbance simulating a BLI.

IPCT is a camera-based method for non-contact measurement of flowed-around structures such as airfoils or propellers, where surface geometry and deformation can be measured relative to the unflowed state. For the reconstruction of surface and deformation, stereoscopic or multi-camera systems as well as photogrammetric methods are often used, which allow to determine the 3d coordinates of the surface by triangulation of corresponding image areas in different views. For this purpose, the surfaces to be examined are coated with a random speckle pattern that allows displacements and deformations to be evaluated with subpixel accuracies using image-based correlation algorithms from particle image velocimetry (PIV).

Brief description of the CRISPMulti test rig

The fan rig is mounted in the two-shaft test facility M2VP of the Institute of Propulsion Technology of the German Aerospace Center (DLR). The CRISPMulti rig consists of 10 blades in the front rotor (R1) and 12 blades in the downstream rotor (R2) with a diameter of about 1m. The blades of the rotors rotate in a 10-to-8 speed ratio. At 100% rotational speed the rig reaches a reduced mass flow of 156kg/s with blade tip speeds exceeding 270m/s at flow Mach numbers at the tip of Ma~1, with IPCT performed only up to 95% speed. An incoming fuselage boundary layer is simulated using a boundary layer distortion grid (see Fig. 1) followed by a honeycomb flow straightener about 3m upstream of the fan. The boundary layer fence can be hydraulically lifted into position at different depths and is fully rotatable around the perimeter such that the instrumentation can measure the displacement effects for different circumferential positions without needing to be traversed.

Implementation of IPCT

To provide a speckle pattern, a single blade of the first rotor was coated with retroreflective micro-glass spheres of 100-300µm diameter embedded in acrylic paint. Due to the retroreflectivity of the micro glass spheres, a large part of the incident light is reflected back to the light-source, which allows imaging of the rotor blade with short exposure times. In addition, the small-scale nature of the speckle structure of the retroreflective coating enables higher accuracies in cross-correlation analysis of displacements in comparison to conventional mm-sized dot patterns as applied by speckle coatings via masking foils [Klinner et al. 2022].
For the transformation of measured deformations into global machine coordinates reference points were placed at 9 positions on the coated blade. These points consist of reflective checkerboard-shaped markers with a size of about 8x8mm². The reference markers (see Fig. 2, right) were printed on self-adhesive film and their surface was sealed additional with a transparent epoxy.

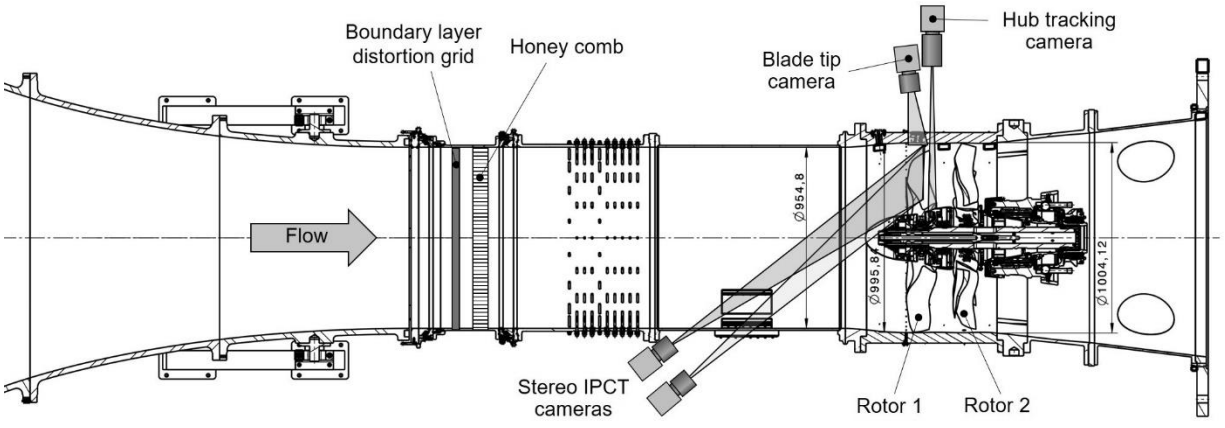

Fig. 1 Overview of the IPCT instrumentation on the CRISPMulti test rig

To determine the marker positions, the blade surface was scanned by an optical 3d measuring arm (Hexagon absolute arm with laser scanner) and mapped onto the CAD model in global machine coordinates.
Stroboscopic illumination of the coated blade surface for each camera was performed with high-power LEDs [Willert et al. 2012]. An aspherical collimator lens (NA=0.63, effective focal length 24mm) projected the emitting area (2.6x3.2mm², OSRAM OSTAR LE CG P2A) onto the blade surface.
Given a maximum rotation speed of up to 5200rpm rotor no. 1 exhibits tip velocities of up to 270m/s (or 270µm/µs) such that flash-based illumination in the single microsecond range is required to keep motion blur acceptable, that is, within a few pixels on the image detector. A recently developed in-house driver electronics for HP-LEDs [Willert 2012, Klinner et al. 2022] reduced the pulse rise time from O(1µs) to 170ns allowing for the generation high intensity light pulses of 1µs duration.
The stereoscopic recording of the suction side of the measuring blade was conducted with two sCMOS cameras with 5MPixels each through two large-area windows located in the upstream pipe section (see Fig. 1), which are located about 1m upstream of the first rotor at circumferential offset of 120° and 187° to the coated blade. The upstream stereo IPCT cameras are equipped with Nikkor 105mm lenses stopped down to f#11 in order to achieve the highest possible depth of field with sufficient scattered light signal. The lenses are placed at working distances (origin of the calibration target to the lens) of 1.9m and 1.7m each.
For the actual measurements a third camera was added to image a reference marker on the hub near the root of the blade (Hub tracking camera in Fig. 1) in order to account for the frame-to-frame jitter, i.e. displacements due to bearing play, shaft torsion and uncertainties in the speed trigger [Klinner et al. 2022].
An additional fourth camera recorded the displacements at the blade tip, allowing additional comparisons with the blade displacements measured with the stereoscopic configuration.
Both, blade tip and hub are simultaneously imaged through two plane windows introduced in the rotor case above rotor 1 with imaging ratios of about 25µm/pixel (Fig. 2, left).
Both cameras (also sCMOS) simultaneously observe a reference pattern on the hub at the root of the IPCT measuring blade (Fig. 2, middle) and a painted pattern consisting of dots and retroreflective paint on the blade tip (Fig. 2, right).
To enable speed-independent imaging at a phase-locked angular position, a microcontroller with a 600MHz clock rate was used as a phase shifter which continuously calculates the frequency of the speed trigger and outputs the corresponding trigger signals for the HP-LEDs and cameras (for details on the phase shifter see also Klinner et al. 2022).

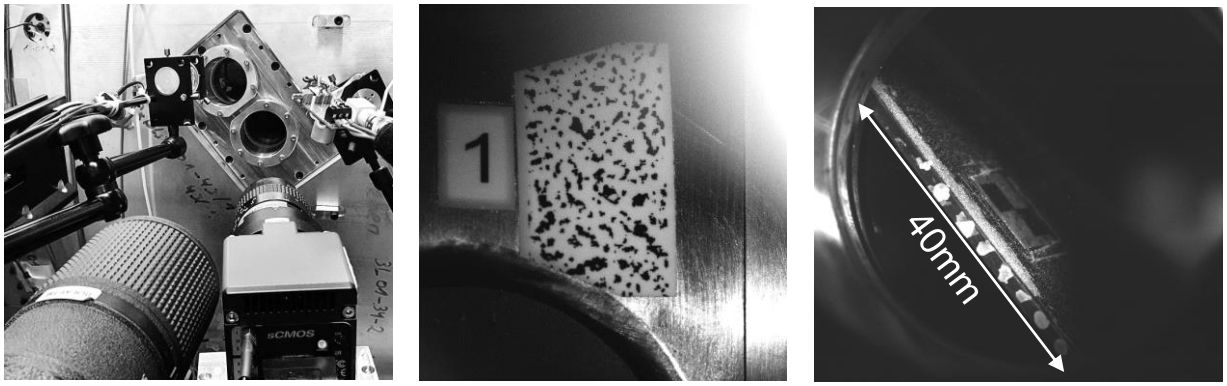

Fig. 2 left: Radial camera setup for simultaneous acquisition of speckle pattern on the hub (center) and near the blade root (right); Center: image of the hub tracking camera; right: simultaneously acquired image of the blade tip with painted dot pattern and reference marker.

All cameras were operated at full image size 2560x2160pixels, also to achieve a uniform delay between image trigger (9956µs) and exposure gate (10-20µs). Cameras were operated in double image mode (PIV mode) required to enable exact triggering of the exposure gate. In order to remain below the maximum possible image transfer rate, image acquisition is performed with a fixed divisor of 2-6 with respect to the rotor speed.

Camera calibration and stereoscopic image processing

The stereo camera setup was calibrated using a 300x150mm² calibration plate with checkerboard pattern, the long side of which was approximately aligned with the leading edge of the blade (see Fig. 3a). During calibration, the plate is mounted inside the shroud using the window plug placed radially above rotor no.1. The holder is designed to minimize the distances between the calibration plate and the area of the curved blade surface visible through the cameras. The corners of the checkerboard pattern were detected with subpixel accuracy and their image coordinates served as point correspondences for the determination of the Tsai camera model [Tsai 87, Willert 2006]. Through the parameters of the camera model, the camera positions were determined relative to the coordinate system of the calibration plate (x_c,y_c with z_c=0). Functions consisting of ratios of second and first order polynomials were chosen as mapping functions between image coordinates and coordinates of the calibration target since these minimized the back-projection error. After image rectification and mapping onto the calibration plane, the imaging ratio of the stereo cameras was 125µm/pixel. The 3d-3c deformation vectors were reconstructed from three speckle-displacement fields obtained from cross-correlation between interrogation windows in four rectified and mapped images, i.e. both reference and displaced images from two stereo views.
Speckle displacements were evaluated using commercial standard 2d-2c cross-correlation software (PIVview 3.9) and an in-house Python-based PIV package for batch processing. Image enhancement is applied to improve speckle image contrast which increases the data validation rate in the subsequent cross-correlation analysis. Here, clipping of intensities above 98% of the cumulative intensity range was applied. To further enhance the pattern contrast and to compensate for spatial variations of illumination, images are high pass filtered by a Gaussian kernel of more than twice the width of the largest structure of the speckle pattern followed by thresholding, binarization and low pass filtering. Using a coarse-to-fine PIV processing algorithm with a final interrogation window size of 32×32pixels (4×4mm² on the reference plane) achieves validation rates near 98% for displacement fields between images of the

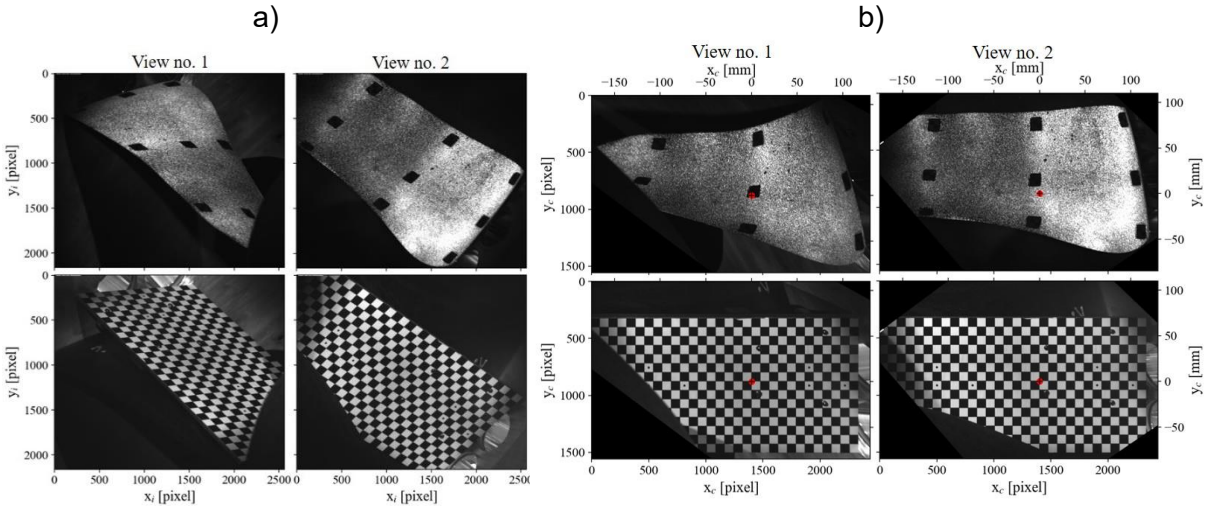

Fig. 3 Stereoscopic reference images at rotor standstill (top) and corresponding calibration images (bottom); a) raw images b) after rectification and mapping onto the calibration plate.

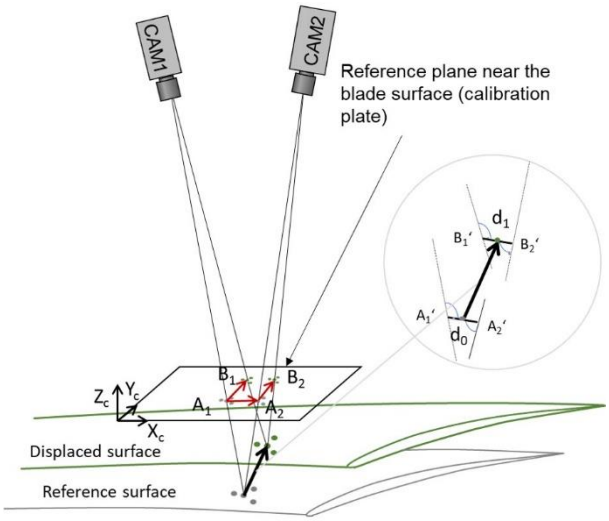

Fig. 4 Reconstruction of 3d-3c deformation vectors by stereo IPCT

reference and deformed blade in similar views. The corresponding validation scheme is based on normalized median filtering with a threshold of 4.0 [Westerweel and Scarano (2005)].

Cross-correlation analysis of the hub-tracking and blade-tip camera images was performed in a similar manner (cf. [Klinner et al. 2022]) and yielded planar displacements at the blade root (hub) and tip.

The reconstruction of both the undeformed surface and the 2d-3c deformation vectors was done by Python based scripting. The undeformed reference surface is recovered from the 2d-2c disparity vector A_1A_2 (see Fig. 4). The corresponding 3d point on the surface is obtained by triangulating the lines of sight passing through the projection centers of the two cameras and the coordinates of A_1 and A_2.The surface point is determined by half of the shortest distance between both line segments d_0 (distance between the 3-d points A_1' and A_2' in Fig. 4). In the best case, both lines of sight intersect on the surface. Measurement uncertainties lead to an increased distance d_0, which is therefore also referred to as triangulation error of undeformed surface in the following. Per interrogation window, the deformation vector is evaluated based on the 2d-2c displacements A_1B_1 and A_2B_2 followed again by triangulating the lines-of sight segments between the projection centers and the coordinates at B_1 and B_2. The corresponding displacement A_2B_2 at A_2 is found by bivariate spline interpolation over a rectangular mesh of displacements evaluated from the 5x5 neighborhood of interrogation windows.

Finally, rigid-body transformation was applied to transfer the stereoscopic measurement data from IPCT measurement coordinates (x_c,y_c,z_c) to the global CAD machine coordinate system (x,y,z). Translation vector and rotation matrix were determined based on eight reference points by least-squares fitting using an algorithm by [Arun et al. 1987] which lead to a residuum of <0.4mm (0.3% of the tip chord length).

Before averaging the individual shots, both the displacements measured stereoscopically and those measured with the tip camera were compensated for frame-to-frame axial and tangential deviations of the reference hub position from displacements simultaneously acquired with the hub tracking camera (cf. Fig. 1).

For both blade tip and stereoscopic measurements, the axial displacement of the hub was directly subtracted. The circumferential hub displacement was scaled by the radius-ratio and subtracted from the circumferential blade tip displacement measured with the tip camera. For compensations of circumferential hub displacements in the stereoscopic data, an angular offset was determined from hub tracking, which was compensated in the 3c displacements by a corresponding counter-rotation around the machine axis.

Finally, all deformations are reduced by deformations at idle speed (15%) to compensate for possible bearing backlash from the blade root.

Stereo matching and restrictions of cross-correlation processing

The stereoscopic reconstruction of the blade surface requires stereo matching between both cameras to assign corresponding image areas that observe the same region on the blade

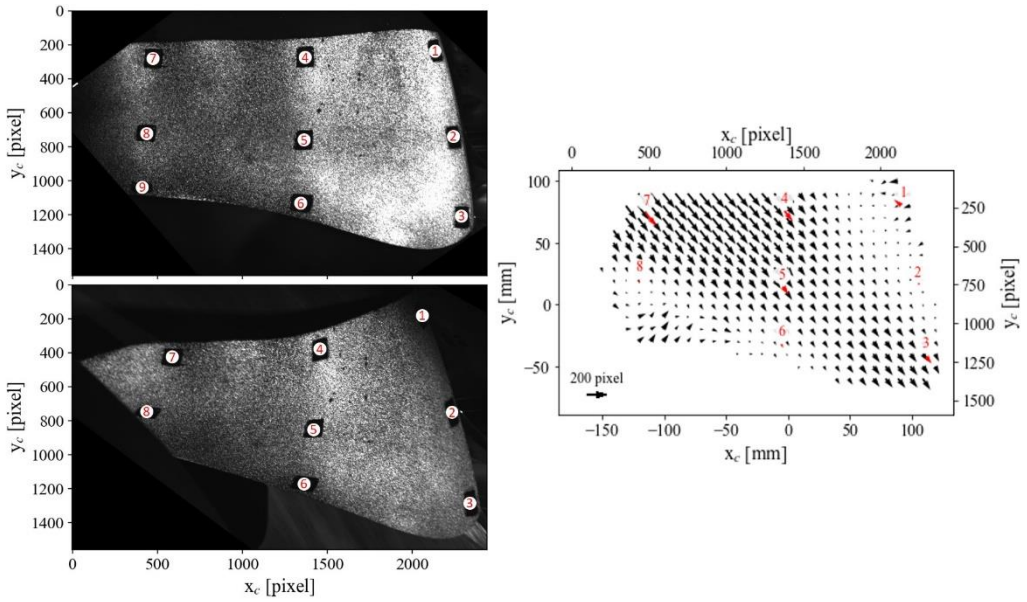

Fig. 5 Mapped stereoscopic views of the blade (left) and result from stereoscopic matching using cross-correlation processing based on a multigrid approach (right); red vectors correspond to reference marker displacements directly evaluated from mapped image coordinates.

surface. For this purpose, correlation-based stereo matching was applied in a first approach similar to a cross-correlation based analysis of camera disparities for stereo PIV.
Since displacement magnitudes up to 12% of the image height occur (up to 170pixels), a coarse-to-fine PIV processing algorithm was applied starting at a window size of 256x256pixels with a final interrogation window size of 64x64pixels. Additionally, an initial predictor field was applied that was averaged from 3 displacement fields evaluated with different fixed integer offsets. The resulting displacement field is shown in Fig. 5 (right), supplemented by the displacements at eight marker positions (red arrows) evaluated directly from their image coordinates. For markers no. 4,5,6,7 the relative absolute deviations to directly evaluated marker displacements in x_c and y_c were below 1%. For marker no. 3 (trailing edge) the relative absolute deviation is 5% along x_c and 9% along y_c.
Since large disparities in stereo matching are also associated with large triangulation errors d_0, the latter is used to reject erroneous regions in the overall dataset.

Validation by blade tip displacement measurements and exemplarily 3d-3c results

To enable a validation of the stereoscopic image processing, axial and circumferential displacements at the blade tip were evaluated additionally from images of the blade tip (cf. Fig. 2, right) and stereoscopically near the marker no. 2 (see Fig. 5, left). Fig. 6 shows a comparison of axial (Δx) and circumferential (Δy) tip displacements for 20 angular positions of the distortion grid as well as for conditions without inlet distortion for both 65% and 85% rotational speed. The Δy-component matches with the displacements obtained from the tip images. The axial Δx-component exhibits maximum deviations on the order of 0.5mm (0.3% of tip chord length) between 100-200° at 65% speed which probably result from slight tilting of one of the cameras during rig operation.
Finally, Fig. 7 shows the recovered mean blade deformations measured at 85% rotational speed (4390rpm) mapped onto the blade geometry with the BL-fence retracted (top row) and with the BL-fence overlapping (middle row) and in opposite angular position with respect to the measuring blade (bottom row). Deformations were reduced by displacements at 15% speed. The *x,y,z* coordinates correspond to the global CAD coordinate system with the *x*-axis

aligned with the rotor axis. Displacements were decomposed in tangential Δt and circumferential Δc components (second and third column in Fig. 7). These displacements result from the respective balance of the centrifugal and compressive forces acting on the blade. One can clearly see the influence of the inlet disturbance on the deformation, which leads to differences exceeding a few millimeters depending on the angular position.

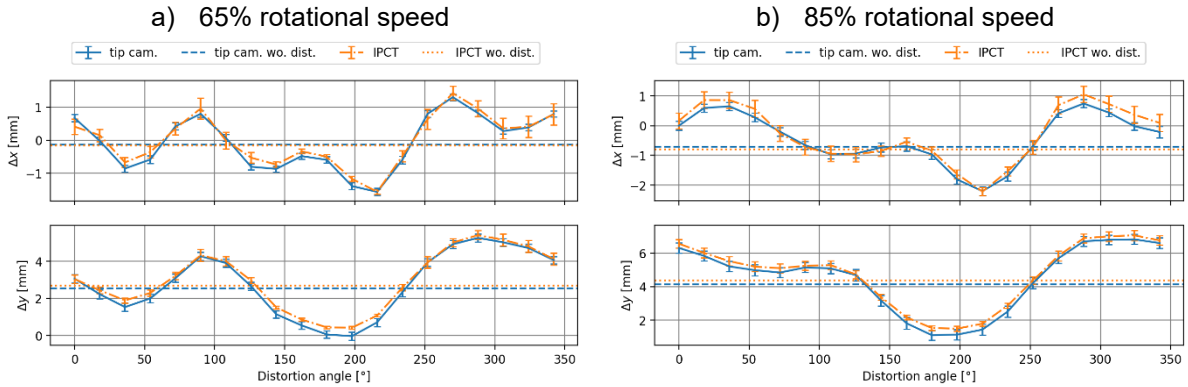

Fig. 6 Axial (top) and circumferential (bottom) variation of the tip displacement as obtained by IPCT of marker no. 2 (see Fig. 2,right and Fig. 5) and blade-tip imaging. Error bars correspond to the rms over 750 snapshots. Dotted or dashed line: test conditions without distortion grid

Conclusions and Outlook

Blade deformation measurements could be realized on a highly loaded double-rotor shrouded fan rig with composite blades. The acquired stereo IPCT data was analyzed using conventional correlation-based algorithms originating from PIV. From planar speckle displacements, the blade surface and their 3d-3c displacements were reconstructed by triangulating the lines-of-sight through corresponding image regions in the stereoscopic views. By compensating the trigger jitter as well as torsion and vibration of the shaft using displacements from simultaneous speckle images of the hub, blade deformations could be obtained with mean triangulation errors below 0.5mm. Comparative measurements using a third camera imaging the blade tip agree well with displacements from stereo IPCT processing within deviations on the order of 0.5mm for the axial component whereby the circumference component matches closely. The measured deformations of the blade subjected to input distortion over one revolution can be further decomposed into harmonic components of the rotor frequency to allow comparisons with modal contributions from forced response calculations.

Literature

Aulich, A.-L., Görke, D., Blocher, M., Nicke, E., & Kocian, F. (2013): „Multidisciplinary automated optimization strategy on a counter rotating fan". In ASME Turbo Expo 2013. American Society of Mechanical Engineers (ASME). DOI: 10.1115/GT2013-94259

Arun, K. S. and Huang, T. S. and Blostein S. D. (1987): "Least-Squares Fitting of Two 3-D Point Sets", *IEEE Transactions on Pattern Analysis and Machine Intelligence*, vol. PAMI-9, no. 5, pp. 698-700, DOI: 10.1109/TPAMI.1987.4767965.

Boden, F. and Stasicki, B. (2014): "Non-intrusive in-flight propeller blade deformation measurements by means of a rotating camera", In ETC2014 - 34. European Telemetry and Test Conference, Nürnberg, 03-05 june, (p. 58 - 63). DOI: 10.5162/etc2014/4.1

Eichner, F., and Belz, J. (2018): "Application of the Modal Approach for Prediction of Forced Response Amplitudes for Fan Blades." ASME. *J. Eng. Gas Turbines Power*. 141(3): 031019. DOI: https://doi.org/10.1115/1.4041453

Kirmse, T., Maring, S., Ebel, P.-B., Schröder, A. (2016): "Fan blade deformation measurements on the DLR Airbus A320-ATRA by means of IPCT as part of the ground test campaign in the frame of the DLR-project SAMURAI" In New Results in Numerical and Experimental Fluid Mechanics X (p. 629-638). DOI: 10.1007/978-3-319-27279-5_55

Klinner, J., Schroll, M., Lengyel-Kampmann, T., Belz, J., Eichner, F., Winkelmann, P., Willert, Christian (2022): "Measurement of Aerodynamically Induced Blade Distortion on a Shrouded Counter-Rotating Prop-Fan" In 20th International Symposium on Application of Laser and Imaging Techniques to Fluid Mechanics, 11.-14. Jul. 2022, Lisbon, Portugal.
Lengyel-Kampmann, T., Karboujian, J., Schnell, R. & Winkelmann, P. (2022): "Experimental investigation of an efficient and lightweight designed counter-rotating shrouded fan stage" In 15th European Turbomachinery Conference, 24-28.April 2023, Budapest
Schmid, T., Lengyel-Kampmann, T., Schmidt, T., & Nicke, E. (2019): „Optimization of a carbonfiber composite blade of a counter-rotating fan for aircraft engines" In 13th European Conference, ETC13. Lausanne, Switzerland. DOI: 10.29008/ETC2019-432
Tsai, R. (1987, August): "A versatile camera calibration technique for high-accuracy 3D machine vision metrology using off-the-shelf TV cameras and lenses". *IEEE Journal on Robotics and Automation*, 3(4), 323–344. DOI: 10.1109/JRA.1987.1087109
Westerweel J and Scarano F (2005): "Universal outlier detection for piv data" *Experiments in Fluids* 39(6):1096–1100. DOI: 10.1007/s00348-005-0016-6.
Willert, C. (2006): "Assessment of camera models for use in planar velocimetry calibration" *Experiments in Fluids*, 41(1), 135–143. DOI:10.1007/s00348-006-0165-2
Willert, C. E., Mitchell, D. M., and Soria, J.(2012): "An assessment of high-power light-emitting diodes for high frame rate schlieren imaging". Experiments in Fluids 53(2):413–421. DOI:10.1007/s00348-012-1297-1.

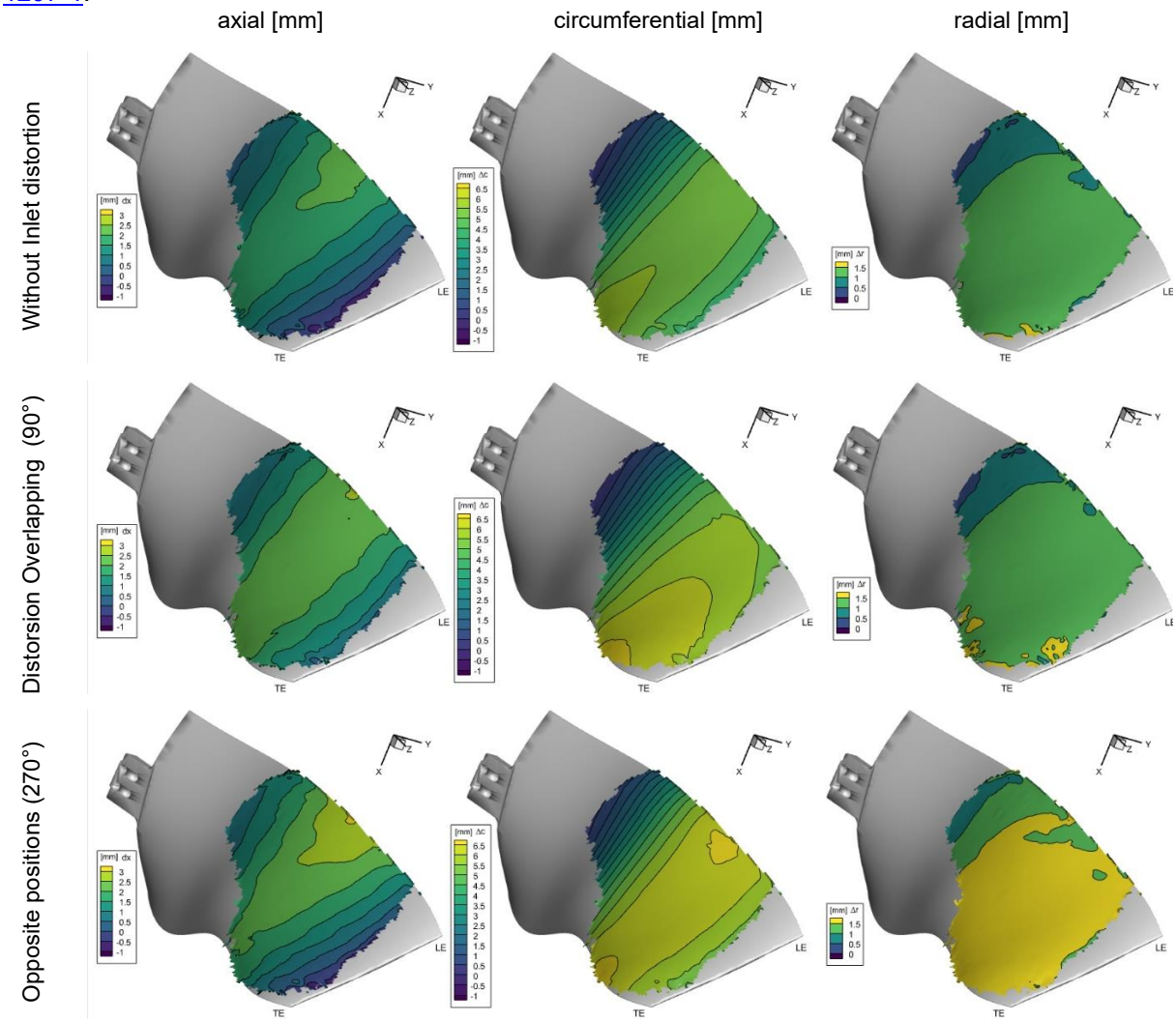

Fig. 7 Axial (left), circumferential (middle) and radial (right) deformations of the rotor blade measured at 85% rotational speed (4390rpm) with respect to idle conditions at 15% speed; top row: without distortion grid, middle row: distortion grid and blade overlapping, bottom row: distortion grid and blade at opposite angular positions. The x-axis corresponds to the machine axis.